



Features of electric field distribution along helium atmospheric plasma jet in stepwise propagation mode of guided streamer

M. E. Pinchuk^{1,a}, G. B. Sretenović^{2,b}, N. Cvetanović^{3,c}, A. A. Dyachenko^{1,d}, B. M. Obradović^{2,e}, and O. M. Stepanova^{1,f}

¹ Institute for Electrophysics and Electrical Power of the Russian Academy of Sciences, Dvortsovaya Naberezhnaya 18, Saint-Petersburg 191186, Russia

² University of Belgrade, Faculty of Physics, Studentski trg 12, Belgrade 111001, Serbia

³ University of Belgrade, Faculty of Transport and Traffic Engineering, Vojvode Stepe 305, Belgrade 111000, Serbia

Received 25 February 2023 / Accepted 26 May 2023 / Published online 16 June 2023

© The Author(s), under exclusive licence to EDP Sciences, SIF and Springer-Verlag GmbH Germany, part of Springer Nature 2023

Abstract. A non-uniform distribution of the electric field along an atmospheric pressure helium plasma jet has been determined using the Stark spectroscopy technique at the stepwise propagation of a guided streamer in a free plasma jet and in the jet interacting with a grounded dielectric target. The plasma jet with guided streamers in the stepwise propagation mode is generated by tailoring applied voltage bunches consisting of a superposition of microsecond bipolar square pulses and damped oscillations. The guided streamer head stops at the oscillating voltage falling slope and then propagates further on the next raising voltage front. The electric field distribution along the jet reflects the dynamics of streamer propagation. The electric field strength decreases at a streamer propagation stagnation phase. The field strengthening at the subsequent raising voltage front accelerates the guided streamer at the second propagation step.

1 Introduction

Atmospheric pressure cold plasma jets are objects of intensive scientific and practical research [1–3]. These plasma sources are attractive due to their capability to be used for processing temperature-sensitive objects in atmospheric air at a distance from the powered electrodes. Several medical devices based on the plasma jets are being tested in clinical practice [4]. Dielectric barrier discharge plasma jets in helium are sort of the most common used cold plasma sources [5].

The successful application of non-equilibrium plasma sources in clinical medical practice is possible only with the precise control of the action on the living object [2,6]. Prospects for the use of plasma jets as ionization sources in mass spectroscopy [7] for the analysis of temperature-sensitive materials, such as biological tissues, are also associated with precise control of the impact of the jet on an object surface. Accordingly, the tasks of the plasma jet design with definite parameters and evaluation of the jet impact with these parameters on the object of treatment arise from this needs [8,9].

A plasma jet in outer air environment is produced by a sequence of ionization waves or guided streamers along a gas flow [10]. The streamer head with a large electric field is the production area for highly active chemical components [11]. In itself, a high electric field can be one of the main acting factors in the treatment of objects [12,13], including living ones. Currently, the combination of an electric field, plasma, and chemical agents on biological objects is being actively investigated by many scientific teams [13,14]. Therefore, determining the electric field profile along the plasma jet is an important task for practical applications. Additionally, it should be noted that the ability to control the propagation of the streamer and, accordingly, the position of the region with a high field is also of considerable interest.

M. E. Pinchuk, G. B. Sretenović, N. Cvetanović and A. A. Dyachenko have contributed equally to this work.

T.I.: Physics of Ionized Gases and Spectroscopy of Isolated Complex Systems: Fundamentals and Applications.

Guest editors: Bratislav Obradović, Jovan Cvetić, Dragana Ilić, Vladimir Srećković and Sylwia Ptasinska

^a e-mail: pinchme@mail.ru (corresponding author)

^b e-mail: sretenovic@ff.bg.ac.rs

^c e-mail: nikola@ff.bg.ac.rs

^d e-mail: dyachenko_180396@rambler.ru

^e e-mail: obrat@ff.bg.ac.rs

^f e-mail: omstepanova@ieeras.ru

The electric field distribution along a free plasma jet in helium and for the jet interacting with a target has the universal nature for a wide range of helium plasma jet sources [5] with nanosecond and microsecond voltage pulses, as well as sinusoidal voltages of various frequencies from several kilohertz up to several tens of kilohertz. A guided streamer passes along the jet length in one cycle without stopping. In case of free expanding plasma jet, the field strength increases monotonically with the jet length up to the certain point where it decreases and diminishes [5, 15], while in case with the target the electric field rises monotonically with the additional field enhancement in the vicinity of the target. The change in velocity and increase of the electric field strength along the length of the jet are associated with an increase in the air concentration in the helium flow [15, 16]. The propagation mode of the streamer can be changed by using a specially tailored voltage. The superposition of bipolar pulses with damped oscillations in voltage pulse bunches makes it possible to obtain a stepwise mode of streamer propagation in a helium plasma jet [17, 18]. The streamer acceleration or its stagnation is directly related to the field in the streamer head [16, 19]. Thus, the behavior of the streamer propagation should be associated with the relevant field redistribution along the jet. In this work, we show the features of the electric field distribution along the free plasma jet and for the interaction of the plasma jet with the dielectric target at stepwise propagation of the guided streamer.

2 Experimental set-up

The plasma jet was directed vertically upward at the helium (99.996%) flow rate of 6.51/min. The scheme of the experimental set-up is shown in Fig. 1. The plasma jet was generated by dielectric barrier discharge in a quartz tube with the inner diameter of 4.6 mm and the thickness of the wall of 1 mm. The inner electrode is made of copper wire of 1.5 mm in diameter placed along the tube axis at the distance of 7.5 mm from the edge of the tube. The outer electrode is made of 5 mm wide copper foil strip wrapped around the tube at the distance of 5 mm from its edge and connected to the ground through a measuring capacitor C_{1m} .

The free plasma jet and the jet interacting with a target were studied. A quartz glass disk 22 mm in diameter and 4 mm thick was used as a target. The distance from the end of the discharge tube to the target surface was 3 cm. A copper plate was placed behind the disk and connected to the ground through a measuring capacitor C_{2m} .

High-voltage tailoring signal is applied to the inner electrode. The high-voltage signal was generated as bunches repeated with a frequency of ≈ 1.8 kHz and duty cycle of $\tau_{\text{bunch}}/T_{\text{bunch}} \approx 55\%$ (Fig. 2). Each bunch was filled with ≈ 45 kHz bipolar square pulses superimposed on them by ≈ 350 kHz damped oscillations. The time uniformity of the high-voltage bunches was evalu-

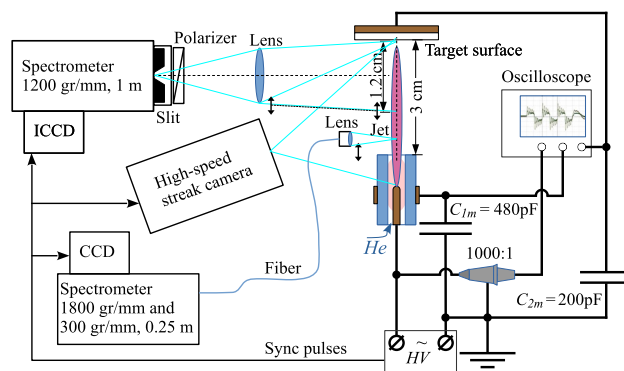


Fig. 1 Schematic overview of the experimental set-up

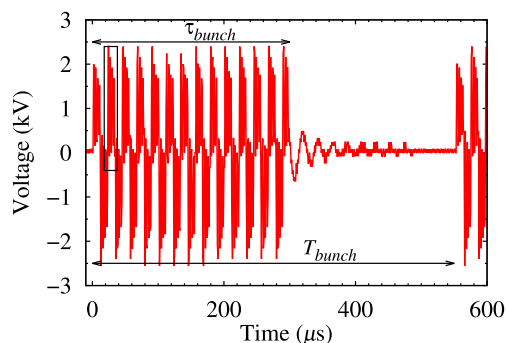


Fig. 2 Voltage signal across the discharge gap with duty cycle $\tau_{\text{bunch}}/T_{\text{bunch}} \approx 55\%$. The rectangle marks the second pulse in which the electric field was determined from the Stark spectroscopy

ated using 50 bunches. The variation in their durations did not exceed 6 ns. The additional details about the electrical arrangement can be found in [18, 20].

The voltage signal across the gas discharge unit was recorded by 1000:1 Tektronix P6015A high voltage divider (Tektronix, USA; bandwidth 75 MHz) and with oscilloscope LeCroy 104Xi oscilloscope (Teledyne LeCroy, USA; bandwidth 500 MHz). The transferred charge through the discharge gap and the target circuit was measured by measuring capacitors $C_{1m} = 480$ pF and $C_{2m} = 200$ pF correspondingly, using 10:1 LeCroy PP007-WR probes (Teledyne LeCroy, USA; bandwidth 500 MHz). Corresponding current signals were obtained by differentiating the smoothed recorded charge waveforms.

The high-speed photochronography (streak imaging) technique, optical emission spectroscopy, and Stark emission spectroscopy were used in this work. A technical description of these techniques is given below in the relevant sections. The high-speed photostreaks presented below were recorded in the experimental series simultaneously with spectral temperature measurements. Stark measurements of field strength were taken in other experimental series, but that the guided streamer dynamics and the signal oscillograms were completely matched together with the previous experiments.

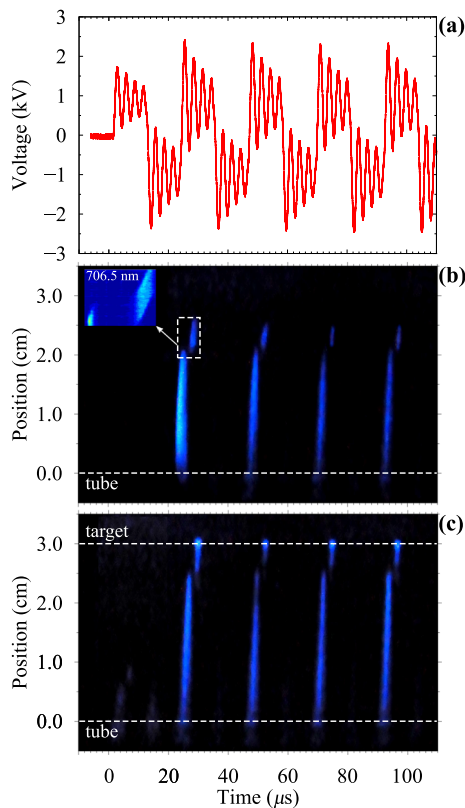


Fig. 3 Voltage across the discharge gap (a) and photostreak of guided streamer propagation in free jet (b) and jet with target (c) for the first five bipolar pulses in the voltage bunch

3 Experimental results and discussions

3.1 Guided streamer dynamics

The behavior of the guided streamer in the jet was determined using high-speed streak imaging. High-speed optical photostreaks were recorded with K-004 streak camera with image intensifier tube (BIFO, Moscow, Russia; sensitivity range 380–800 nm, recording sweep speed from 0.1 ns/cm to 300 ms/cm with sweep length of 4 cm). High-speed photostreaks obtained by the time strobing method, with 30 accumulations, produced each in a new voltage bunch.

Features of the streamer propagation are clearly visible in photostreaks. Photostreaks in the full range of camera sensitivity at the first five bipolar pulses synchronized with the voltage signal for a free jet and a jet with a target are shown in Fig. 3. A more detailed streamer propagation to the surface target in the second positive voltage pulse is presented in Fig. 4. Photograph of the plasma jet is shown in Fig. 4c for comparison with the streak image. A stepwise propagation of a guided streamer is observed both for the free plasma jet and the plasma jet interacting with target. At the positive front of the voltage pulse, the guided streamer starts from the tube along the helium flow. Further, the streamer head

stops at the voltage drop phase and then propagates further on the next voltage oscillation front. Subframes, inserted in Figs. 3b and 4d, demonstrate the streamer dynamics near the position of the intermediate stop of the streamer at a wavelength of the helium line of 706.5 nm. Streak images at 706 nm were obtained with 10,000 gate accumulations. Thus, the streamer moves in two steps in each positive voltage pulse. At the applied voltage, the streamer reaches the target surface at the second propagation step for the jet with the target. In this case, the plasma jet covers a greater distance in the presence of the target than the length of the free plasma jet. In the second step, the streamer head accelerates from less than 5 to over 30 km/s as it approaches the target. The streamer touching the target matches the current spike through the target and the characteristic break slope in the charge curve. Time matching of the target touching the current spike is marked by the vertical arrow in Fig. 4c, d.

The streamer propagation dynamics is reproduced from pulse to pulse, except for the first voltage pulse in the voltage bunch. Measurements were taken for a long time continuously for up to several hours. The streamer dynamics is shown to be a regular process with high repeatability.

3.2 Integral spectra and temperature profile along plasma jet

Optical spectra were recorded along the length of the plasma jet automatically. The radiation was collected by a quartz lens onto the optical fiber connected to an MS-257 spectrograph (LOT-Oriel, Germany; fiber optic 50 μm, 1800 gr/mm grating blazed at 500 nm, resolution of approx 0.1 nm, and 300 gr/mm grating blazed at 500 nm) with a CCD camera DU-420-UV-FK (Andor tech., UK; pixels: 1024x256). The radiation-collecting unit with the lens was moved along the jet by a micropositioner with a step motor controlled by a microcontroller with computer management. The unit passage was with intermediate interval stops determined by the computer program, for recording spectra in the stop positions. The spectra were taken from a spatial region of 1 mm in diameter with exposure time of 1 sec with averaging by 8 accumulations. The spectrograph was calibrated using spectral lamps LOT-Oriel 60xx series. The spectral intensities were corrected using spectra records of the calibrated spectral irradiance standard lamp LOT-Oriel 6358, geometrically placed as the jet discharge. The irradiance corrected spectra of the plasma jet with target in three position at 1, 2 and 3 (near target surface) cm from tube orifice are shown in Fig. 5. The intensities in Fig. 5a were normalized to the maximum at 391 nm, observed near the target surface. The transverse size of the jet was comparable to the size of the light collection area. The cross section distribution of the jet parameters was not considered.

Molecular bands of N_2 , N_2^+ , OH and oxygen, hydrogen, helium lines were observed in the plasma jet spectrum in range of 300–800 nm. The intensity profiles

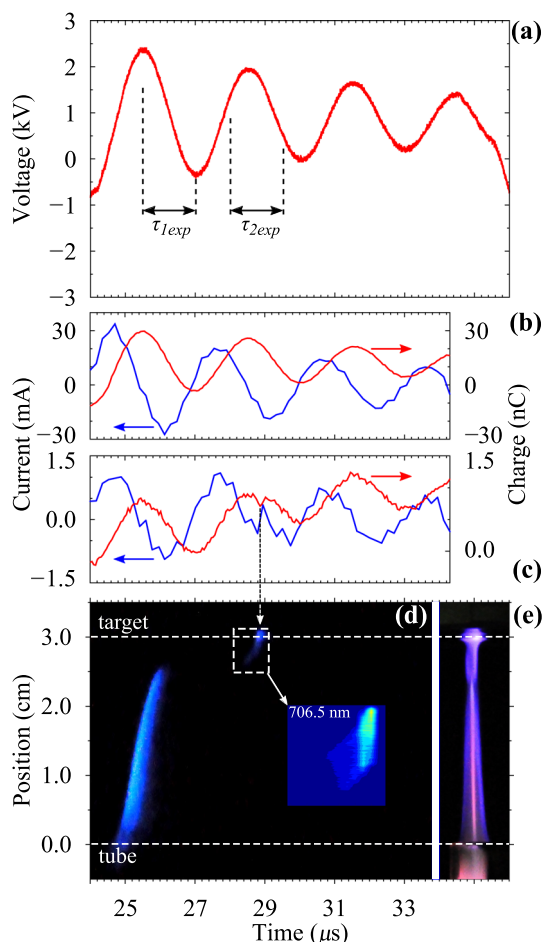


Fig. 4 The voltage across the discharge gap (a); current and charge through the discharge tube circuit (b) and target circuit (c); photostreak (d) of guided streamer propagation to the target at the second positive voltage pulse in the bunch. Integral photo of the jet (e). Time matching of the streamer touching the target to the current spike through the target is marked by the vertical arrow from (c) to (d). Time marks in (a) show exposure time for Stark spectra recording

with 30 data record points (10 recording positions per 1 cm) along the plasma jet, normalized to the maximum at 391 nm near the target surface, are shown in Fig. 6 for several plasma components. An increase in the intensity of the oxygen and nitrogen radiation reflects a monotonic increase in the air content in the gas flow. The intensity of helium emission lines is strongly dependent on the electron temperature in the range of 2–10 eV [21], which is typical for helium plasma jet [5, 10]. The electron temperature in this range is a function of the reduced electric field [22]. Adjusted for the violation of the correspondence of the line intensity to the field due to the interaction of helium molecules with impurity molecules, the emission intensity of the He 706.5 nm line can be interpreted as the qualitative behavior of the averaged electric field in the streamer head as it passes along the jet [23].

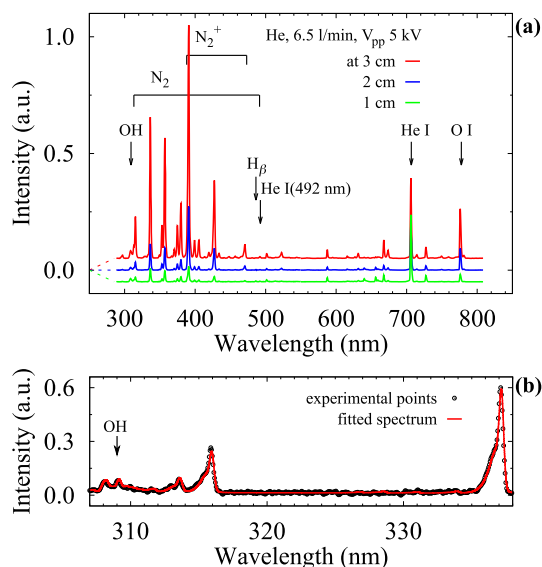


Fig. 5 Optical spectra (a) of plasma jet with target at different positions 1, 2, and 3 cm from tube orifice. Example of a fitted spectrum (b) for the spectrum at 3 cm in (a) for temperature determination. The tube orifice is zero position, and the target surface is set at 3 cm

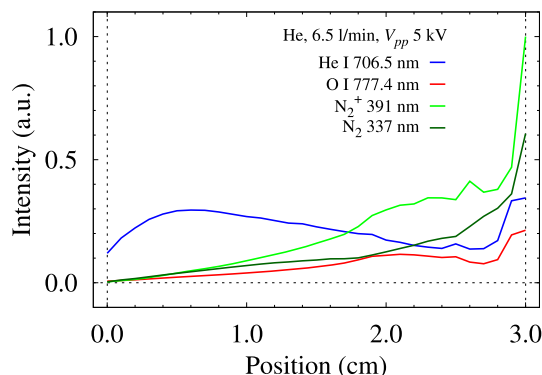


Fig. 6 Normalized radiation intensity at 706.5(He), 777.4(O), 391(N₂⁺) and 337(N₂) nm along the plasma jet. The tube orifice is zero position, and the target surface is set at 3 cm

The plasma temperature along the plasma jet was measured by analyzing the profiles of the N₂ Second Positive System C³Π–B³Π (SPS). The data were processed by the MassiveOES program [24, 25]. The process consists of approximating the experimental spectrum with a model one (see Fig. 5b) taking into account the contribution of N₂ C–B and OH A–X bands in spectral range 304–338 nm. The temperatures of the levels of N₂ molecules were chosen as simulation parameters. The dependencies of the vibrational and rotational temperatures in N₂ C–B band versus position are shown in Fig. 7. The errors in Fig. 7 were determined from statistics using a nonlinear least squares solver in the MassiveOES program. The rotational temperature profile reflects the cooling of the gas downstream. The main energy release occurs in the discharge tube. The energy

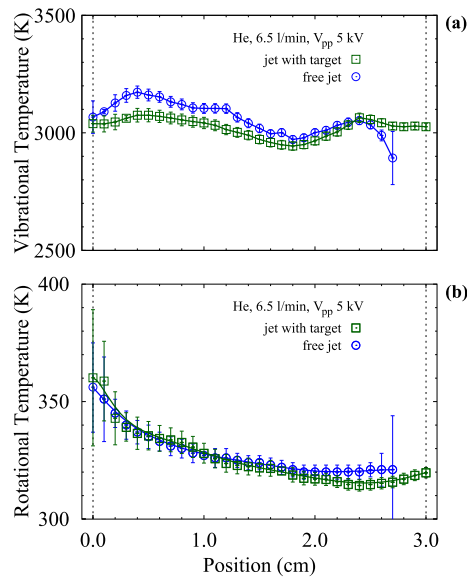


Fig. 7 Rotational temperature in N_2 SPS spectral band along plasma jet for free jet and jet with target. The tube orifice is zero position, and the target surface is set at 3 cm

released in the streamer channel is much lower than in the discharge tube.

3.3 Electric field along plasma jet

For the electric field measurements [26], projection optics was used to project the upper part of the plasma jet onto the entrance slit of a 1 m spectrometer with 1200 gr/mm diffraction grating (Minuteman Lab. Inc., USA). Entrance slit width was 50 μm . Radiation from the jet was polarized in the axial electric field direction (π -polarization) using polarizer and detected using an ICCD (PI-MAX2, Princeton Instruments, USA; pixels: 1024x256). ICCD was triggered using time delayed pulse signal from the start time of the high-voltage bunch. The ICCD gate was triggered during the first and second oscillation of the second positive pulse in the bunch. The gate exposure time was 1.5 μs as marked in Fig. 4a. This camera preset provided independent determination of electric field in the streamer at the first streamer propagation step and at the second one. The intensity of He line at 492.2 nm was very weak. Consequently, each recorded image is made of 10 accumulations, each of 50,000 or 100,000 gates per exposure.

The size of the observable image for 1 m spectrometer was limited by the height of its entrance slit. Due to this limitation, the electric field could not be measured over the entire jet length, but only over a region 1.2 cm long, see Fig. 1. The observed jet region (projected onto the entrance slit) was chosen by shifting the jet vertically, thereby keeping the plasma in the focal plane (see Fig. 1). In such a way, to determine the field, two most interesting regions were chosen for both jets. The first is the position of the intermediate stop of the streamer, and the second is at the end of the jet plume. The mea-

sured electric field value corresponds to the propagation of the streamer head in the exposure time window. This value should be close to the peak field value in particular position. An example of the ICCD spectral image with subsequent spectra fitting is shown in Fig. 8.

The π -polarized spectrum in the vicinity of He I 492.19 nm was fitted in order to determine the electric field strength from the wavelength shift of the allowed and forbidden component. The method is used here, which was already successfully applied on a various DBD discharges, including jet discharge, see in [26] and references therein. It uses an overall fitting function that includes the allowed (4D), forbidden (4F) and the non-shifted field-free component (ff). Here, specifically, there is a significant intensity of nitrogen molecular band C–B(1–7) at 491.68 nm, belonging to the second positive system (SPS), and it had to be included in the fitting function, see Fig. 8a. Due to the overlap of the field-free and the wide allowed component, the mathematical fitting procedure had to be adapted, so that it relies predominantly on the forbidden component. This was done because the forbidden line is only emitted in the presence of strong electric field and therefore it is not influenced by the excitation of the surrounding gas—out of the streamer head. Therefore, the position of the forbidden component was set as the highest dependable parameter while the position and intensity of the allowed and field free component only increase the quality of the fit and accuracy of the obtained field value. Accordingly, this fitting procedure requires the knowledge of exact position of the non-shifted (field-free) line, and the position of N_2 band in the measured spectrum. The temperature value was used as parameter in calculation the nitrogen band shape. Similar mathematical procedure had to be used in an atmospheric pressure RF discharge due to its complex geometry of the plasma sheath [27]. The Stark shifts of the π -components were taken from [28]. The tabulated wavelength and shape of N_2 SPS were taken from software MassiveOES [24, 25] and data [29], while the positions of N_2 band and He I in the measured spectrum were obtained using Geissler tube, geometrically placed as the jet discharge. In the present case, the field is not strong enough to induce a detectable splitting of the spectral line [26, 28]. Thus, the He I line shapes are taken as Pseudo-Voigt, typical for DBD discharges, taking into account all important line broadening mechanisms: instrumental, van der Waals, resonant and Doppler. From the numerical standpoint, the overall fitting function is formed as a single function by adding up spectral profiles of the four abovementioned components: $f(\lambda) = \text{He4D}(\lambda) + \text{He4F}(\lambda) + \text{Heff}(\lambda) + \text{N}_2(\lambda)$, see Fig. 8. Curve fitting was performed using Matlab's [30] nonlinear least-squares solver with the trust-region reflective algorithm. Free parameters are the components' intensities and the electric field strength, while line widths are allowed to vary only within the expected values. It should be noted that in Fig. 8, separate components are plotted only for illustration, while the actual fitting is performed with a single function $f(\lambda)$. The uncertainty of the field value comes from the

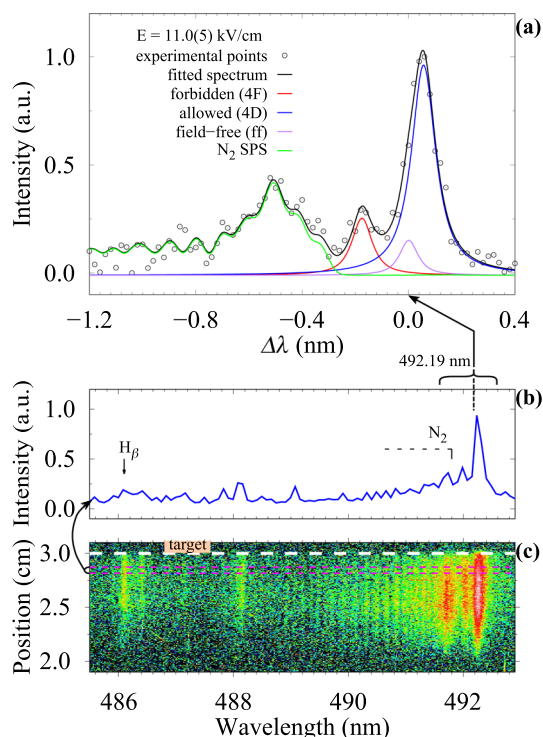


Fig. 8 Example of a fit (a) for spectral components at 492.19 nm in spectra (b) in the ICCD spectral image (c) near the target surface

uncertainty of the fit. To increase the signal-to-noise ratio, the fitting procedure was carried out for the signal obtained by averaging ten consecutive vertical pixel strips in the original spectral image, see arrow from (c) to (b) in Fig. 8.

The measured electric field distribution is given in Fig. 9 for the case of the free jet and the jet with dielectric target. It should be noted that the region for spectroscopic field measurement was limited only to a section of the streamer, due to the relatively large length of the jet compared to the entrance slit of the spectrometer. Therefore, these regions for spectroscopic field measurement are displaced by some distance relative to each other for the free jet and the jet with the target in Fig. 9. We turned our attention to measuring the field at the instance where jet streamer stops and subsequently propagates (transition from step 1 to 2). Specifically, in both cases the region around the middle of the jet was examined. It should be noted that in both cases the experimental uncertainty of the electric field is significant, due to the low intensity of the He I 492.19 nm and the emission out of the strong field region. For the jet with target the electric field development exhibits a clear increase of the strength toward the target. Similar values and distribution shape were obtained with PVC target in [31]. It is evident in the graph that the electric field strength continues its distribution after the jet stops with a slight increase of values from the first to the second step. For the free jet, the field distribution is different, but again, it is clear that the streamer devel-

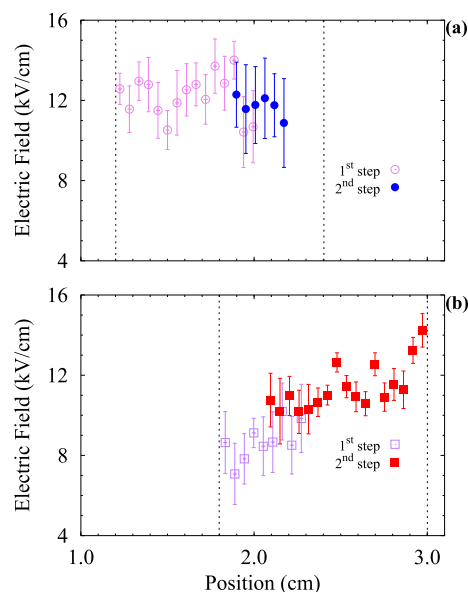


Fig. 9 Electric field along free jet (a) and jet with target (b) at stepwise streamer propagation. The vertical dash lines show the boundaries of the measurement regions

opment continues after the stop, with a small increase of the electric field strength from step 1 to 2. This can be expected as the streamer is reignited in a preionized channel with a somewhat reduced electron density.

The admixture of air to helium and the electric field in the streamer head mainly determine the streamer dynamics [5, 15, 16]. The field is related to the head potential and is indirectly determined by the applied voltage value. At a pulsed voltage with a duration of $\approx 1 \mu\text{s}$, the potential of the streamer head at streamer stagnation is indicated $\approx 2 \text{ kV}$ for pure helium with an increase proportional to the air impurity content [16]. In our cases, the mean air content of 2–4% at the intermediate streamer stop position $\approx 2 \text{ cm}$ [32] corresponds to the stopping potentials of 2.2–2.4 kV in [16]. This is very close to our voltage amplitude of 2.5 kV, especially taking into account the voltage decrease in the voltage oscillations. According to [5, 15] the field required for streamer movement must be higher than 5 kV/cm in the guided streamer head in pure helium flow, with the necessary increase for further propagation in the presence of an air impurity. This field value was also noted as a threshold for a strong increase of helium line emission.

In our jet, the field in the head is close to the threshold field required for the streamer propagation [22]. A decrease in the field to 10–8 kV/cm corresponds to a streamer deceleration in the stagnation phase at the first step of the streamer's propagation at the falling slope of the applied voltage oscillation, see Figs. 3, 4, and 9. At the growing voltage front, the field increases to 10–12 kV/cm, which allows the streamer to move further without stopping in the helium flow with air content. The values of the field for deceleration and acceleration of the streamer in the free jet and the jet

with the target differ due to the significant difference in the hydrodynamics of the flows, and the corresponding distribution of the concentration of air impurity for these two cases.

In this work, we have shown a specific case for the given experimental parameters. But the applied voltage waveform, its amplitude, and the gas flow rate change the dynamics of the guided streamer in the jet [33]. A transition from stepwise propagation to propagation in one pass is determined by the applied voltage and gas flow rate [32]. The streamer's intermediate stop position in stepwise mode can be smoothly moved by changing the oscillation frequency in voltage pulses [34] and the gas flow rate [32]. Apparently, the field distribution along the jet follows the change in the dynamics of the streamer propagation. The stepwise guided streamer propagation at an applied voltage with nanosecond pulses was also observed in [35], and a non-monotonic field distribution along the jet was also obtained for that case [35]. Thus, in plasma jets, it is possible to change the electric field distribution by tailoring the applied voltage waveform. This may be useful in practical applications.

4 Conclusion

The non-uniform distribution of the electric field along the plasma jet was determined using the Stark spectroscopy technique at the stepwise propagation of the guided streamer in the free plasma jet and in the jet interacting with the grounded dielectric target. The stepwise propagation of a guided streamer was recorded with tailoring applied voltage bunches consisting of a superposition of microsecond bipolar square pulses and damped oscillations. The stepwise propagation mode of the ionization wave in the gas flow was observed for positive voltage pulses in the bunches. The streamer head stops at the oscillating voltage falling slope and then propagates further on the next raising voltage front. The electric field strength decreases at a streamer propagation stagnation phase. On the contrary, the field strengthening at the subsequent raising voltage front accelerates the guided streamer at the second propagation step. In the presence of the target, an increase in the field near the target surface is observed.

Acknowledgements The study was financially supported by the Russian Science Foundation (project 22-29-01215, <https://rscf.ru/en/project/22-29-01215/>). The authors would like to thank Ministry of science, technology development and innovations of the Republic of Serbia for the technical support for the research.

Author contributions

MP led the project. MP, GS, NC and AD put forward the idea of the research and conceived the experiments.

MP, GS, NC and AD conducted the experiments. All authors analyzed and discussed the data and results. MP and OS wrote the draft manuscript. All authors reviewed the manuscript. All authors have read and agreed to the published version of the manuscript.

Data Availability Statement This manuscript has no associated data or the data will not be deposited. [Authors' comment: The data that support the findings of this study are available within the article. Additional data that support the findings of this study are available from the corresponding author upon request.]

Declarations

Conflict of interest The authors declare no conflicts of interest.

References

1. I. Adamovich, S.D. Baalrud, A. Bogaerts, P.J. Bruggeman, M. Cappelli, V. Colombo, U. Czarnetzki, U. Ebert, J.G. Eden, P. Favia, D.B. Graves, S. Hamaguchi, G. Hieftje, M. Hori, I.D. Kaganovich, U. Kortshagen, M.J. Kushner, N.J. Mason, S. Mazouffre, S.M. Thagard, H.-R. Metelmann, A. Mizuno, E. Moreau, A.B. Murphy, B.A. Niemira, G.S. Oehrlein, Z.L. Petrovic, L.C. Pitchford, Y.-K. Pu, S. Rauf, O. Sakai, S. Samukawa, S. Starikovskaia, J. Tennyson, K. Terashima, M.M. Turner, M.C.M. van de Sanden, A. Vardelle, The 2017 plasma roadmap: low temperature plasma science and technology. *J. Phys. D Appl. Phys.* **50**(32), 323001 (2017). <https://doi.org/10.1088/1361-6463/aa76f5>
2. I. Adamovich, S. Agarwal, E. Ahedo, L.L. Alves, S. Baalrud, N. Babaeva, A. Bogaerts, A. Bourdon, P.J. Bruggeman, C. Canal, E.H. Choi, S. Coulombe, Z. Donkó, D.B. Graves, S. Hamaguchi, D. Hegemann, M. Hori, H.-H. Kim, G.M.W. Kroesen, M.J. Kushner, A. Laricchiuta, X. Li, T.E. Magin, S. Mededovic Thagard, V. Miller, A.B. Murphy, G.S. Oehrlein, N. Puac, R.M. Sankaran, S. Samukawa, M. Shiratani, M. Šimek, N. Tarasenko, K. Terashima, E. Thomas Jr, J. Trieschmann, S. Tsikata, M.M. Turner, I.J. van der Walt, M.C.M. van de Sanden, T. von Woedtke, The 2022 plasma roadmap: low temperature plasma science and technology. *J. Phys. D Appl. Phys.* **55**(37), 373001 (2022). <https://doi.org/10.1088/1361-6463/ac5e1c>
3. X. Lu, P.J. Bruggeman, S. Reuter, G. Naidis, A. Bogaerts, M. Laroussi, M. Keidar, E. Robert, J.-M. Pouvès, D. Liu, K.K. Ostrikov, Grand challenges in low temperature plasmas. *Front. Phys.* (2022). <https://doi.org/10.3389/fphy.2022.1040658>
4. H.-R. Metelmann, T. von Woedtke, K.-D. Weltmann, *Comprehensive Clinical Plasma Medicine*, 1st edn. (Springer, Berlin, 2018). <https://doi.org/10.1007/978-3-319-67627-2>
5. P. Viegas, E. Slikboer, Z. Bonaventura, O. Guaitella, A. Sobota, A. Bourdon, Physics of plasma jets and interaction with surfaces: review on modelling and experiments. *Plasma Sources Sci. Technol.* **31**(5), 053001 (2022). <https://doi.org/10.1088/1361-6595/ac61a9>

6. A. Jurov, S. Kos, T. Blagus, I. Sremački, G. Filipič, N. Hojnik, A. Nikiforov, C. Leys, M. Čemažar, G. Serša, U. Cvelbar, Atmospheric pressure plasma jet-mouse skin interaction: Mitigation of damages by liquid interface and gas flow control. *Biointerphases* **17**(2), 021004 (2022). <https://doi.org/10.1116/6.0001596>
7. K. McKay, T.L. Salter, A. Bowfield, J.L. Walsh, I.S. Gilmore, J.W. Bradley, Comparison of three plasma sources for ambient desorption/ionization mass spectrometry. *J. Am. Soc. Mass Spectrom.* **25**(9), 1528–1537 (2014). <https://doi.org/10.1007/s13361-014-0924-x>
8. T. von Woedtke, S. Emmert, H.-R. Metelmann, S. Rupf, K.-D. Weltmann, Perspectives on cold atmospheric plasma (cap) applications in medicine. *Phys. Plasmas* **27**(7), 070601 (2020). <https://doi.org/10.1063/5.0008093>
9. L. Lin, D. Yan, T. Lee, M. Keidar, Self-adaptive plasma chemistry and intelligent plasma medicine. *Adv. Intell. Syst.* **4**(3), 2100112 (2022). <https://doi.org/10.1002/aisy.202100112>
10. X. Lu, G.V. Naidis, M. Laroussi, K. Ostrikov, Guided ionization waves: theory and experiments. *Phys. Rep.* **540**(3), 123–166 (2014). <https://doi.org/10.1016/j.physrep.2014.02.006>
11. X. Lu, G.V. Naidis, M. Laroussi, S. Reuter, D.B. Graves, K. Ostrikov, Reactive species in non-equilibrium atmospheric-pressure plasmas: generation, transport, and biological effects. *Phys. Rep.* **630**, 1–84 (2016). <https://doi.org/10.1016/j.physrep.2016.03.003>
12. S.A. Krivov, A.V. Lazukin, Y.A. Serdyukov, S.V. Gundareva, G.A. Romanov, Effect of constant high-voltage electric field on wheat seed germination. *IOP SciNotes* **1**(2), 024002 (2020). <https://doi.org/10.1088/2633-1357/aba1f6>
13. P. Huang, L. Xu, Y. Xie, Biomedical applications of electromagnetic detection: a brief review. *Biosensors* **11**(7), 225 (2021). <https://doi.org/10.3390/bios11070225>
14. A. Lazukin, M. Pinchuk, A. Korsukova, A. Nikiforov, G. Romanov, O. Stepanova, O. Grabelnyh, Comparison of presowing wheat treatments by low-temperature plasma, electric field, cold hardening, and action of tebuconazole-based disinfectant. *Appl. Sci.* **12**(13), 6447 (2022). <https://doi.org/10.3390/app12136447>
15. G.B. Sretenović, I.B. Krstić, V.V. Kovačević, B.M. Obradović, M.M. Kuraica, The isolated head model of the plasma bullet/streamer propagation: electric field-velocity relation. *J. Phys. D Appl. Phys.* **47**(35), 355201 (2014). <https://doi.org/10.1088/0022-3727/47/35/355201>
16. M. Hofmans, P. Viegas, O. van Rooij, B. Klarenaar, O. Guaitella, A. Bourdon, A. Sobota, Characterization of a khz atmospheric pressure plasma jet: comparison of discharge propagation parameters in experiments and simulations without target. *Plasma Sources Sci. Technol.* **29**(3), 034003 (2020). <https://doi.org/10.1088/1361-6595/ab6d49>
17. M.E. Pinchuk, O.M. Stepanova, A.M. Astafiev, A.V. Lazukin, Z. Chen, Stepwise propagation of a guided streamer along a dbd helium plasma jet fed by biased oscillating voltage. *Appl. Phys. Lett.* **114**(19), 194103 (2019). <https://doi.org/10.1063/1.5099968>
18. M. Pinchuk, A. Nikiforov, V. Snetov, Z. Chen, C. Leys, O. Stepanova, Role of charge accumulation in guided streamer evolution in helium DBD plasma jets. *Sci. Rep.* **11**, 17286 (2021). <https://doi.org/10.1038/s41598-021-96468-4>
19. X. Li, B. Guo, A. Sun, U. Ebert, J. Teunissen, A computational study of steady and stagnating positive streamers in N₂-O₂ mixtures. *Plasma Sources Sci. Technol.* **31**(6), 065011 (2022). <https://doi.org/10.1088/1361-6595/ac7747>
20. O.M. Stepanova, O.V. Rybalchenko, M.E. Pinchuk, A.M. Astafiev, O.G. Orlova, V.A. Spodobin, A.A. Kudryavtsev, Bactericidal effect of a dielectric barrier discharge plasma jet generated in laminar and preturbulent helium flows. *Plasma Med.* **7**(3), 187–200 (2017). <https://doi.org/10.1615/PlasmaMed.2017019064>
21. L.C. Johnson, E. Hinnov, Electron temperatures from He I intensity measurements. *Phys. Fluids* **12**(9), 1947–1949 (1969). <https://doi.org/10.1063/1.1692765>
22. Y.P. Raizer, *Gas Discharge Physics* (Springer, Berlin, Heidelberg, 1991)
23. Q. Xiong, X. Lu, J. Liu, Y. Xian, Z. Xiong, F. Zou, C. Zou, W. Gong, J. Hu, K. Chen, X. Pei, Z. Jiang, Y. Pan, Temporal and spatial resolved optical emission behaviors of a cold atmospheric pressure plasma jet. *J. Appl. Phys.* **106**(8), 083302 (2009). <https://doi.org/10.1063/1.3239512>
24. J. Voráč, P. Synek, L. Potočnáková, J. Hnilica, V. Kudrle, Batch processing of overlapping molecular spectra as a tool for spatio-temporal diagnostics of power modulated microwave plasma jet. *Plasma Sources Sci. Technol.* **26**(2), 025010 (2017). <https://doi.org/10.1088/1361-6595/aa51f0>
25. J. Voráč, P. Synek, V. Procházka, T. Hoder, State-by-state emission spectra fitting for non-equilibrium plasmas: OH spectra of surface barrier discharge at argon/water interface. *J. Phys. D Appl. Phys.* **50**(29), 294002 (2017). <https://doi.org/10.1088/1361-6463/aa7570>
26. B.M. Obradović, N. Cvetanović, S.S. Ivković, G.B. Sretenović, V.V. Kovačević, I.B. Krstić, M.M. Kuraica, Methods for spectroscopic measurement of electric field in atmospheric pressure helium discharges. *Eur. Phys. J. Appl. Phys.* **77**(3), 30802 (2017). <https://doi.org/10.1051/epjap/2017160479>
27. Z. Navrátil, R. Josepson, N. Cvetanović, B. Obradović, P. Dvořák, Electric field development in γ -mode radiofrequency atmospheric pressure glow discharge in helium. *Plasma Sources Sci. Technol.* (2016). <https://doi.org/10.1088/0963-0252/25/3/03lt01>
28. N. Cvetanović, M.M. Martinović, B.M. Obradović, M.M. Kuraica, Electric field measurement in gas discharges using Stark shifts of He I lines and their forbidden counterparts. *J. Phys. D Appl. Phys.* **48**(20), 205201 (2015). <https://doi.org/10.1088/0022-3727/48/20/205201>
29. R.W.B. Pearse, A.G. Gaydon, *The Identification of Molecular Spectra* (Springer, Dordrecht, 1976)
30. MATLAB: Version 9.3 (R2017b). The MathWorks Inc., Natick, Massachusetts (2017)
31. M. Hofmans, A. Sobota, Influence of a target on the electric field profile in a khz atmospheric pressure plasma jet with the full calculation of the stark shifts. *J. Appl. Phys.* **125**(4), 043303 (2019). <https://doi.org/10.1063/1.5075544>

32. M.E. Pinchuk, Z. Chen, O.M. Stepanova, Transition from one-pass mode to stepwise propagation of a guided streamer along a helium plasma jet. *Appl. Phys. Lett.* **119**(5), 054103 (2021). <https://doi.org/10.1063/5.0053672>
33. M.E. Pinchuk, O.M. Stepanova, M. Gromov, A. Nikiforov, Control of guided streamer propagation and interaction with substrate in helium atmospheric pressure plasma jet. *Publ. Astron. Obs. Belgrade* **102**, 163 (2022)
34. M.E. Pinchuk, A.M. Astafev, R.A. Aznabaev, O.M. Stepanova, Applied voltage waveform suitable to control parameters of dielectric barrier discharge plasma jet. *Publ. Astron. Obs. Belgrade* **99**, 225–228 (2020)
35. S. Shen, J. Yan, Y. Wang, Y. Wang, W. Ding, G. Sun, Stepwise development of atmospheric pressure plasma jet driven by bursts of high-voltage nanosecond pulses at multi-tens MHz. *Plasma Sources Sci. Technol.* **31**(10), 105003 (2022). <https://doi.org/10.1088/1361-6595/ac9080>

Springer Nature or its licensor (e.g. a society or other partner) holds exclusive rights to this article under a publishing agreement with the author(s) or other rightsholder(s); author self-archiving of the accepted manuscript version of this article is solely governed by the terms of such publishing agreement and applicable law.